Scripta Materialia 108 (2015) 56–59

Contents lists available at ScienceDirect

Scripta Materialia

journal homepage: www.elsevier.com/locate/scriptamat

Early cluster formation during rapid cooling of an Al–Cu–Mg alloy: In situ small-angle X-ray scattering

P. Schloth [a,b], A. Menzel [c], J.L. Fife [c], J.N. Wagner [d,1], H. Van Swygenhoven [b,d], J.-M. Drezet [a,*]

[a] Ecole Polytechnique Fédérale de Lausanne, Computational Materials Laboratory, Station 12, 1015 Lausanne, Switzerland
[b] Ecole Polytechnique Fédérale de Lausanne, Neutrons and X-rays for Mechanics of Materials, 1015 Lausanne, Switzerland
[c] Paul Scherrer Institut, Swiss Light Source, 5232 Villigen PSI, Switzerland
[d] Paul Scherrer Institut, Materials Science and Simulation, ASQ/NUM, 5232 Villigen PSI, Switzerland

ARTICLE INFO

Article history:
Received 21 April 2015
Revised 3 June 2015
Accepted 13 June 2015
Available online 15 June 2015

Keywords:
Aluminum alloys
Solute clustering
Quenching
Vacancies
Small-angle X-ray scattering

ABSTRACT

The formation of Cu–Mg clusters in an Al–Cu–Mg aluminum alloy is observed by small-angle X-ray scattering during cooling. Cooling rates are choosen to mimic the different conditions obtained at the surface and in the center of large forgings. Clusters of 0.45 nm start to form at 250 °C. Their volume fraction depends strongly on the cooling rate and the amount of excess vacancies. The difference in cluster kinetics explains the difference in rapid hardening across large forgings.

Age-hardenable Al–Cu–Mg alloys are widely used for aerospace and engineering applications owing to their high specific strength and good corrosion resistance. Their age hardening response is characterized by two distinct stages. The first stage is defined by a fast initial increase in strength, which is known as rapid hardening. It was shown by 3D atom probe tomography (APT) and small-angle X-ray scattering (SAXS) experiments that the rapid hardening is associated with the formation of Cu–Mg clusters [1–4]. The second rise to peak hardness is generally ascribed to the formation of the equilibrium S phase (Al_2CuMg) [4,5].

For industrial applications, the Al–Cu–Mg alloys are commonly processed as large components such as forgings or plates. The mechanical properties are tailored by the age-hardening treatment, which also involves a quenching step. Thermal gradients decrease from the surface to the center and give rise to residual stresses (RS) [6]. The magnitude of the as-quenched RS can be very high and even exceed the as-quenched strength of the materials [6,7]. In the case of Al–Zn–Mg–Cu alloys, the high as-quenched RS are caused by the formation of fine hardening precipitates that form during quenching of large components and thereby increase the yield strength of the material [8,9].

In order to predict the RS formation in industrial components during quench, the changes of the nanostructure during cooling conditions close to industrial practice needs to be characterized as they highly impact the yield strength and thus the internal stress generation. Further, the influence of excess vacancies on precipitation during cooling needs to be explored. This can be done by adapting the cooling rates at high temperature, which influence the excess vacancy concentration due to annihilation on defects.

SAXS is a useful tool to monitor precipitation phenomena during fast time and temperature changes given that a sufficiently high electron density contrast between the precipitate and matrix exists [4,8,10]. SAXS provides the means to collect information on the size and volume fraction of the precipitates that can then be directly compared to predictions of thermodynamic-based precipitation models [11,12]. These models can be coupled with macroscopic finite-element RS simulations to better predict the residual stress formation during the processing of industrial components [9,13] as part of through-process modeling.

This work investigates the Cu–Mg cluster formation during cooling conditions close to industrial quenching in an Al–Cu–Mg alloy. In addition, a cooling profile with faster rates at high temperature is performed in order to investigate the influence of excess vacancies on the Cu–Mg cluster formation.

A commercial aluminum AA2618 alloy of composition Al-1.9–2.7 Cu-1.3–1.8 Mg-0.9–1.3 Fe-0.9–1.2 Ni-0.1–0.25 Si (wt%) was

* Corresponding author.
[1] Present address: Karlsruhe Institute of Technology, KNMF and IAM-WK, 76344 Eggenstein-Leopoldshafen, Germany.

http://dx.doi.org/10.1016/j.scriptamat.2015.06.015
1359-6462/

used for this study. The specimens feature a size of 3 × 25 × 0.5 mm. The samples were solutionized for 1 h at 525 °C in a salt bath and quenched in water to dissolve residual precipitation. The SAXS experiments were performed at the cSAXS beamline of the Swiss Light Source (SLS) at the Paul Scherrer Institut (PSI), Villigen Switzerland, at a wavelength of 0.774 Å (16 keV) with a beam size of 200 × 200 μm^2. The range of accessible momentum transfers was 0.007 Å^{-1} ⩽ q ⩽ 1 Å^{-1}. A laser-based heating system was used to apply the different heat treatments [14]. The particular setup is explained in more detail in reference [8]. SAXS distributions were recorded every 0.5 s to monitor the dynamic processes during quenching. Before each quench, the samples were solution treated for 7 min at 525 °C to homogenize the microstructure.

The intensity for each scattering vector was azimuthally averaged since the 2D SAXS images revealed isotropic scattering for all scattering angles. The detector images recorded during the quench from solutionizing to room temperature were averaged over 100 equidistant temperature segments ($\Delta T \approx 4.25$ K) to enhance the measurement statistics. The scattering spectra at the solutionizing temperature was used for background subtraction, and the absolute intensity, I, was normalized using glassy carbon as a secondary standard [15]. The cluster size was characterized using a self-consistent Guinier approximation [16]. The average cluster size is equal to the Guinier radius (R_g) when the size distribution of the clusters features a dispersion of 0.2 [16]. The uncertainty on the Guinier radius was calculated from the error associated with the slope of the linear Guinier fit. The scattering invariant (Q) of the clusters was extrapolated from a q-value of 0.05 Å^{-1} to 0 to subtract the scattering due to the S phase at low q-values and from 0.8 to infinity using the Porod asymptote. The volume fraction, f_v, was calculated from the scattering invariant as $Q = \int I(q)q^2dq = 2\Pi^2(\Delta\rho)^2 f_v(1-f_v)$ assuming two phases that are separated by a sharp interface. $\Delta\rho$ is the difference in the electron density between the matrix and the clusters. The scattering vector q is defined as, $q = 4\Pi/\lambda \sin(2\theta/2)$, where λ is the wavelength and 2θ the scattering angle. The chemical composition of the Cu–Mg clusters was taken as 2/3 Mg, 1/3 Cu (at.) [3,4] to calculate the electron density contrast. The uncertainties of the volume fraction calculations cannot be expected to be better than ±10% due to the uncertainties related to the absolute intensity calibration, the extrapolations of the data to 0 and infinity, and the assumptions of the chemical composition of the clusters [17]. The number density of clusters was estimated by assuming spherical clusters as $N = f_v/\left(4/3\Pi R_g^3\right)$.

To investigate the influence of excess vacancies on the cluster formation, the changes of the vacancy site fraction during quenching were estimated. The equilibrium vacancy site fraction $c_{v,eq}$ was calculated using the modified Lomer equation $c_{v,eq} = A\exp(-H_0/(RT))\{1 - 13(c_{Cu} + c_{Mg}) + 12c_{Cu}\exp(E_{Cu\text{-}v}/(RT)) + 12c_{Mg}\exp(E_{Mg\text{-}v}/(RT))\}$ as proposed in reference [18]. In this equation, R is the universal gas constant, H_0 the enthalpy of vacancy formation, c the concentration of Cu and Mg atoms, and E the binding energy between these atoms and vacancies. The values of these parameters were estimated from literature: the enthalpy of formation was taken as 72.24 kJ/mol, and the binding energies between vacancies and Cu and Mg atoms were assumed to be 19.29 and 24.08 kJ/mol, respectively [19,20]. The condensation rate of the concentration of excess vacancies c_v was calculated as, $\partial c_v/\partial t = -(c_v - c_{v,eq})/\tau$ where τ is the characteristic time ($\tau = (l/2\pi)^2/D_v$) [20]. The characteristic diffusion length l for vacancy annihilation was assumed to be equal to the average grain size of 40 μm, considering only grain boundaries as sinks for vacancies. The diffusion of vacancies D_v defined as, $D_v = C_E a^2 \exp(-H_m/RT)$ where C_E is the Einstein constant, a is the lattice parameter and H_m the migration energy of the vacancies.

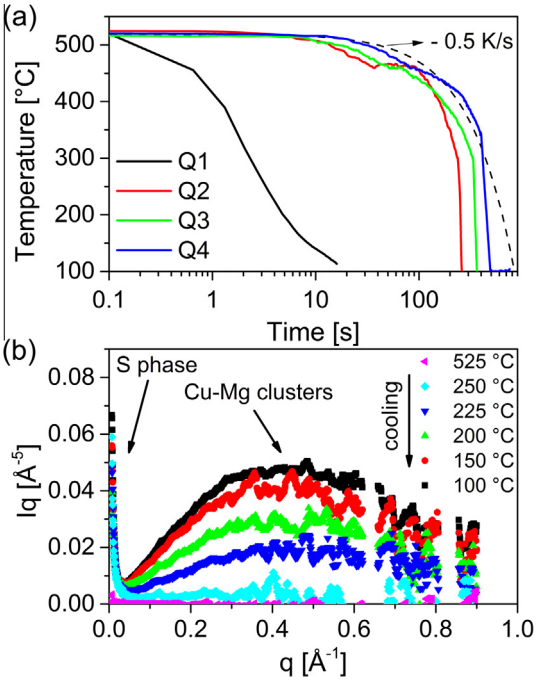

Fig. 1. (a) Cooling curves of the four quench conditions. The dashed black line represent the cooling with a constant rate of −0.5 K/s. (b) Selected Kratky plots (Iq^2 vs. q) as function of temperature for the slowest cooling condition Q4.

A vacancy migration energy of 55.86 kJ/mol was considered, which is within the range of values reported for Al–Cu alloys (41–66.9 kJ/mol) [21].

Fig. 1a shows the four cooling conditions Q1–Q4 that were applied to the specimens. The fastest quench Q1 is similar to the cooling rates close to the surface of a thick plate. The slower quench conditions (Q2–Q4) refers to cooling conditions that are typical between the surface and center of larger forgings [13,20]. The cooling conditions end at 100 °C since large components are often quenched in boiling water to control RS [6].

Fig. 1b shows the evolution of the SAXS signal in the Kratky representation (Iq^2 vs. q) during the Q4 cooling, which is also a representative scattering plot for the other four cooling conditions. At the solutionizing temperature, no scattering effects are observed because the scattering curve at the solutionizing temperature was used for the background subtraction. During cooling, scattering effects are first evidenced at low q-values, indicating the presence of large objects. These objects corresponds to the equilibrium S phase, which precipitates between 410 °C and 300 °C in the AA2618 alloy [13]. The solute loss in the peak aged T6 state due to the formation of S phase is negligible when cooling rates are higher than −0.5 K/s [13]. The applied cooling conditions Q1–Q4 are similar or faster than this critical rate (Fig. 1a) and therefore the anisotropic scattering of the S phase was not observed in the 2D SAXS images.

Further cooling leads to an increasing scattered intensity at high q-values around 0.4 Å^{-1}, which is characteristic for Cu–Mg clusters [4]. The scattering of Cu–Mg clusters appears around 250 °C and increases as the temperature decreases to 100 °C. The volume fraction starts to increase around 250 °C for the four cooling conditions. For the slower cooling rates (Q2–Q4) the rate of volume fraction increase decreases when the temperature gets below 170 °C and seems to reach a plateau, as shown in Fig. 2a. The value reached at 100 °C is highest (2.7%) for Q4 and lowest (0.5%) for Q2. This relates to the cooling rates in the temperature range where Cu–Mg clusters are formed, which is the highest for Q2 (−15 K/s)

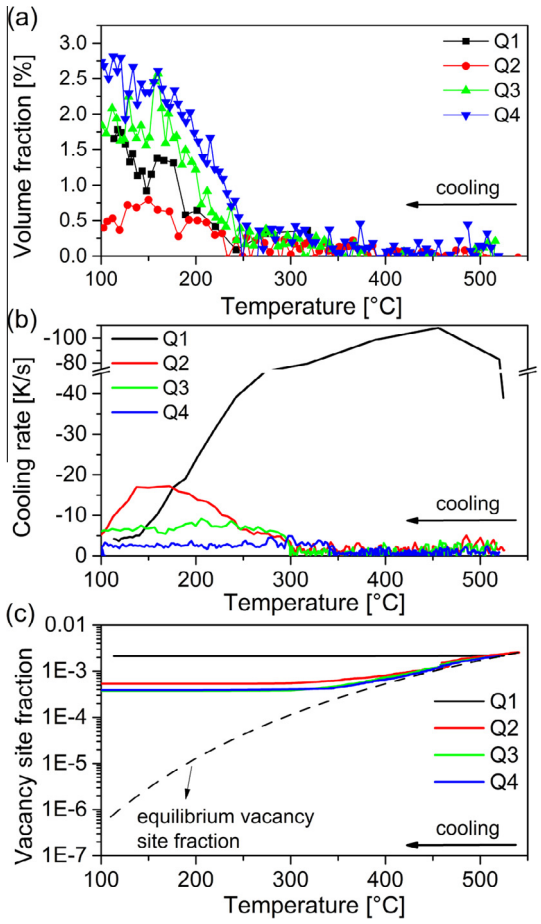

Fig. 2. Evolution of (a) the volume fraction of Cu–Mg clusters, (b) the cooling rates (note the break in the *y*-scale from −45 to −75 K/s) and (c) the vacancy site fraction during the four cooling conditions as function of temperature. The dashed black lines represents the equilibrium vacancy site fraction in (c).

and the lowest for Q4 (−2.5 K/s). The volume fraction of Cu–Mg clusters increases with slower cooling rates as expected when longer precipitation time is provided.

In spite of the larger scattering on the data obtained during the fastest cooling rate (Q1), which mimics cooling conditions at the surface of a thick plate, the results obtained suggest a different behavior of the volume fraction. The increase in volume fraction is slightly shifted to lower temperatures and seems not to flatten when lower temperatures are reached. However, at the end of the cooling profile, the volume fraction of Q1 is similar to Q3 (1.8%) although the cooling rate of Q1 is considerably higher, especially between 240 and 150 °C. This behavior can be related to the vacancy concentrations.

At high temperature, the cooling rates of Q2–Q4 are very similar and in the range of −0.5 to −1.5 K/s as illustrated in Fig. 2c. In contrast, the fast quench of Q1 reaches cooling rates of up to −110 K/s at high temperature. Below 325 °C, the cooling rate of Q1 decreases consistently from −80 K/s to −5 K/s at 150 °C. The high cooling rates of Q1 prevent the annihilation of vacancies as shown in Fig. 2c. In contrast, the slow cooling rates at high temperature for Q2–Q4 lead to an annihilation of vacancies and a smaller amount of excess vacancies. Below 300 °C, in the temperature range where the Cu–Mg clusters form, the vacancy site fraction stays roughly constant for Q1–Q4, but is considerably higher for Q1. An increased amount of excess vacancies increases the solute diffusion [20,22] and therefore the cluster kinetics. This explains why the volume fraction of Q1 is similar to Q3 at the end of the quench, although the cooling rates of Q1 are much higher.

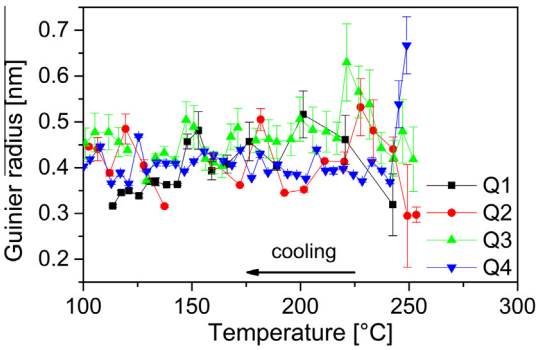

Fig. 3. Evolution of the Guinier radius of the Cu–Mg clusters as function of temperature for the cooling conditions Q1–Q4.

Within the scatter of the data, the Guinier radii of the Cu–Mg clusters that form during quenching is very similar for the four cooling conditions as illustrated in Fig. 3. The Guinier radius stay roughly constant as the temperature decreases and is in the range of ~0.35 nm (Q1) to ~0.5 nm (Q3) at the end of the quenching. This refers to a cluster number density in the range of $2 \cdot 10^{25}$ m^3 (Q2) to $1 \cdot 10^{26}$ m^3 (Q1), which corresponds reasonably well with the cluster densities reported in references [3,4].

Deschamps et al. reported that Cu–Mg clusters with a radius of ~0.45 nm and a volume fraction of 2% (with a likely range of 1.2–3.5%) are responsible for the rapid hardening response in this alloy [4]. The Cu–Mg clusters that form during the different applied cooling conditions feature similar radii and volume fractions except in Q2, which shows a much smaller volume fraction. Therefore when quenching large industrial components, rapid hardening should already take place during quenching and will vary across the cross section of the component depending on the local cooling conditions. The rapid hardening during quench increases the yield strength by cluster strengthening [2] and influences the residual stress formation [13]. Therefore, the Cu–Mg cluster formation needs to be taken into account in the simulation of residual stresses by precipitation modeling [11,12].

In summary, in situ small-angle X-ray scattering experiments performed during rapid cooling of AA2618 at cooling rates mimicking industrial quenching conditions show the formation of nano-sized Cu–Mg clusters. The Cu–Mg cluster formation starts around 250 °C. The radius ranges between 0.35 and 0.5 nm and seems to be independent of the cooling rates. However, the kinetics of the cluster formation and the volume fraction reached are strongly dependent on the cooling rate. As a consequence, rapid hardening is to be expected during quenching and its dependence on cluster volume fraction will be responsible for the formation of residual stresses.

The research was funded by the Competence Center for Materials Science and Technology (CCMX, http://www.ccmx.ch/) involving EPF Lausanne, PSI Villigen, Univ. de Bretagne Sud Lorient, Constellium CRV (725 rue Aristide Bergs, 38400 Voreppe, France) and ABB Turbo Systems Ltd (Bruggerstrasse 71a, 5401 Baden, Switzerland). We thank ABB Turbocharger for providing the material.

References

[1] S.P. Ringer, K. Hono, T. Sakurai, I.J. Polmear, Scrip. Mater. 36 (5) (1997) 517–521.
[2] S. Ringer, T. Sakurai, I. Polmear, Acta Mater. 45 (9) (1997) 3731–3744.
[3] R. Marceau, G. Sha, R. Ferragut, A. Dupasquier, S. Ringer, Acta Mater. 58 (15) (2010) 4923–4939, http://dx.doi.org/10.1016/j.actamat.2010.05.020. <http://linkinghub.elsevier.com/retrieve/pii/S1359645410002958>.

[4] A. Deschamps, T. Bastow, F. de Geuser, A. Hill, C. Hutchinson, Acta Mater. 59 (8) (2011) 2918–2927, http://dx.doi.org/10.1016/j.actamat.2011.01.027. <http://linkinghub.elsevier.com/retrieve/pii/S1359645411000334>.
[5] J. Silcock, J. Inst. Metals 89 (6) (1961) 203–210.
[6] J. Robinson, D. Tanner, C. Truman, Strain 50 (3) (2014) 185–207.
[7] N. Chobaut, J. Repper, T. Pirling, D. Carron, J.-M. Drezet, in: Hasso Weiland, Anthony D. Rollett, William A. Cassada (Eds.), Proceedings of the 13th International Conference on Aluminum Alloys (ICAA13), No. EPFL-CONF-186767, 2012, pp. 285–291.
[8] P. Schloth, J.N. Wagner, J.L. Fife, A. Menzel, J.-M. Drezet, H. Van Swygenhoven, Appl. Phys. Lett. 105 (10) (2014), http://dx.doi.org/10.1063/1.4894768. <http://scitation.aip.org/content/aip/journal/apl/105/10/10.1063/1.4894768>.
[9] N. Chobaut, D. Carron, S. Arséne, P. Schloth, J.-M. Drezet, J. Mater. Process. Technol. 222 (2015) 373–380.
[10] S. Ibrahimkutty, P. Wagener, A. Menzel, A. Plech, S. Barcikowski, Appl. Phys. Lett. 101 (10) (2012), http://dx.doi.org/10.1063/1.4750250. <http://scitation.aip.org/content/aip/journal/apl/101/10/215 10.1063/1.4750250>.
[11] M. Perez, M. Dumont, D. Acevedo-Reyes, Acta Mater. 56 (9) (2008) 2119–2132.
[12] M. Starink, S. Wang, Acta Mater. 57 (8) (2009) 2376–2389.
[13] N. Chobaut, Measurements and Modelling of Residual Stress During Quenching of Thick Heat Treatable Aluminium Components in Relation to Their Precipitation State (Ph.D. thesis), EPFL (THÉSE Nô 6559 (2015), <http://infoscience.epfl.ch/record/205768>).
[14] J.L. Fife, M. Rappaz, M. Pistone, T. Celcer, G. Mikuljan, M. Stampanoni, J. Synchroton Radiat. 19 (3) (2012) 352–358 (225).
[15] F. Zhang, J. Ilavsky, G.G. Long, J.P.G. Quintana, A.J. Allen, P.R. Jemian, Metall. Mater. Trans. A 41 (2010) 1151–1158, http://dx.doi.org/10.1007/s11661-009-9950-x.
[16] A. Deschamps, F. De Geuser, J. Appl. Crystallogr. 44 (2) (2011) 343–352, http://dx.doi.org/10.1107/S0021889811003049. <http://scripts.iucr.org/cgi-bin/paper/S0021889811003049>.
[17] A. Deschamps, F. Geuser, Metall. Mater. Trans. A 44 (1) (2012) 77–86, http://dx.doi.org/10.1007/s11661-012-1435-7. <http://link.springer.com/10.1007/s11661-012-1435-7>.
[18] H.-G. Fabian, R. Wolter, Cryst. Res. Technol. 26 (1) (1991) 93–102.
[19] H. Kimura, A. Kimura, R. Hasiguti, Acta Metall. 10 (6) (1962) 607–619 (245).
[20] D. Godard, Influences de la precipitation sur le comportement thermomecanique lors de la trempe d'un alliage Al–Zn–Mg–Cu (Ph.D. thesis), Institut National Polytechnique de Lorraine Nancy, 1999, URL <http://cat.inist.fr/?aModele=afficheN&cpsidt=198244>.
[21] S. Hirosawa, T. Sato, J. Yokota, A. Kamio, Mater. Trans. JIM 39 (1) (1998) 139–146.
[22] J. Embury, R. Nicholson, Acta Metall. 13 (4) (1965) 403–417, http://dx.doi.org/10.1016/0001-6160(65)90067-2. <http://www.sciencedirect.com/science/article/pii/0001616065900672>.